Bifunctional Polyoxometalates for Planar Gold Surface Nanostructuration and Protein Immobilization

Dimitri Mercier, Souhir Boujday, Cyrine Annabi, Richard Villanneau, Claire-Marie Pradier, Anna Proust

Bifunctional Polyoxometalates for planar gold surface nanostructuration, and protein immobilization

Dimitri Mercier[1], Souhir Boujday[2,3], Cyrine Annabi[2,3], Richard Villanneau[1], Claire-Marie Pradier[2,3], and Anna Proust[1,4*]*

[1] Institut Parisien de Chimie Moléculaire, UMR CNRS 7201, UPMC Univ Paris 06, Université Pierre et Marie Curie, 4 place Jussieu, Case 42, 75252, Paris Cedex 05, France.

[2] UPMC Univ Paris 06, UMR CNRS 7197, Laboratoire de Réactivité de Surface, F75005 Paris, France

[3] CNRS, UMR 7197, Laboratoire de Réactivité de Surface, F75005 Paris, France

[4] Institut Universitaire de France, 103 Bd Saint-Michel, 75005 Paris, France.

RECEIVED DATE ()

Figures (5)

Laboratoire de Réactivité Surface, UMR CNRS 7197, Université Pierre et Marie Curie- Paris 06, 4 Place Jussieu, 75252 Paris cedex 05, France

Tel: +33144276001, Fax: +33144276033, souhir.boujday@upmc.fr, anna.proust@upmc.fr

ABSTRACT

Surface nanostructuration was successfully achieved by binding the polyoxometalate (POM) $(NBu_4)_3[PW_{11}O_{39}\{(SiC_6H_4NH_2\}_2O)]$ covalently onto planar gold surfaces. To do so, POMs, functionalized with two terminal amino groups, were synthesized and let react with a mercaptoundecanoic acid self assembled monolayer adsorbed on gold. These amine-terminated POM macroanions proved to be remarkably efficient as nanostructuring agents. Using Polarization Modulated- Infrared Reflection Absorption Spectroscopy (PM-IRRAS), Photoelectron Spectroscopy (XPS), as well as Atomic Force Microscopy (AFM), conditions were optimized to elaborate a dense and well-dispersed layer of POMs, leaving a "free" amine function for the further linkage of proteins. Anti-rabbit immunoglobulins (anti-rIgGs) were thus grafted on the POM-structured layer and the recognition of their specific target, rabbit immunoglobulin (rIgGs), was tested by using Quartz Crystal Microbalance with dissipation measurement (QCM-D). The recognition was good and highly specific, indicating that an efficient, nanostructured, biosensor has been constructed. The method reported herein can be easily applied, not requiring any sophisticated experimental setup, and is promising for the patterning of any molecular probes bearing amine groups.

Key words: Polyoxometalate, Surface nanostructuration, XPS, QCM-D, AFM, Biosensors.

1. INTRODUCTION

In the competitive context of detection and quantification of biological targets, biosensors are promising alternative to conventional analytical techniques.[1] However, while biosensors enable rapid and low cost analyses, their selectivity and sensitivity still require improvement. Due to its conductive and reflective properties, gold is often used as a transducer surface, allowing electrochemical and/or optical detection. The biological receptor is often immobilized on gold *via* alkylthiols [2,3] or diazonium[4,5] attachment layers. The control of the chemistry and organization of this interface at the nano-level is of crucial importance for the number, the orientation, and the accessibility of the bioreceptors.[6-10] Surface nanostructuration is a way to optimize these parameters. Typically, lithographic techniques enable surface patterning with a resolution below 50 nm.[11-15] Tips of atomic force microscopes, or electron-beam lithography are very elegant, but rather sophisticated tools to modify self-assembled monolayers with a precision at the nanolevel.[16,17] Eventually, the use of colloids, either gold [18,19] or oxide [20] nanoparticles has also proved to be an efficient nanostructuration method in the 5 to 100 nm range. There is thus a crucial need for versatile and easily applicable methods to enable patterning and controlled reactivity of surfaces at the nanometric resolution.

For this purpose, the potential of polyoxometalates (POMs) as nanostructuring agents deserves to be addressed. POMs are discrete nano-scale oxo-clusters of the early transition metals, which display a great variety of molecular structures.[21,22] These molecular oxides are unmatched in terms of properties and related applications.[23,24] POMs synthesis and characterization have reached a level of maturity that should enable their integration in more elaborated materials and devices [25,26]. Due to their anionic character, they have generally been dispersed or immobilized on various supports through electrostatic interactions.[27-30] Several types of POM-based sensors have been described often relying on the redox properties of POMs.[28,31,32] On the other hand, very few results have been reported on the covalent immobilization of POMs on surfaces.[30,33-35] This work thus reports some surface organization of organic-inorganic hybrid POMs, opening new possible functionalities. On the other side, deposition of POMs on HOPG or metallic surfaces have proved to lead to self-assembled 2D-ordered arrays of POMs,[36-40] with well-established applications in electro-assisted catalysis.[41] In a very recent publication, it was even shown that 3D nanostructures could be obtained by drop casting of POM-based compounds and fine control of surface wetting conditions.[42] In this context, the covalent approach should improve the formation of stable, dense and well ordered monolayers, with increased processability; it however requires the controlled functionalization of POMs, namely the availability of some organic-inorganic hybrid POMs, that some of us are thoroughly investigating[26,43-45] and that display appropriate reactive residues to be subsequently grafted to the surface.[30,33-35] In view of application in the biosensor field, bifunctionalized POMs,

with suitable geometry, are required both to achieve surface nanostructuration and to act as anchorage platforms for biological receptors. A single example of heterobifunctionalized POMs is described in the literature, but their separation is not trivial[30] We have thus chosen to tether the homobifunctionalized $[PW_{11}O_{39}\{(SiC_6H_4NH_2)_2O\}]^{3-}$ anion to gold surface substrate pre-covered with mercaptoundecanoic acid. Characterization of the sequential steps of immobilization has been carried out by PM-IRRAS, AFM, and XPS. Eventually, a protein (an antibody) was bound to the nanostructured layer *via* pending amine groups; the covalent binding mode was interrogated by PM-IRRAS and XPS surface analysis and the bioactivity of the so-immobilized antibodies was checked by measuring the molecular recognition of their specific antigen using QCM-D. Figure 1 shows the successive steps of surface nanostructuration using POMs, and the model biosensor elaboration.

Figure 1

2. EXPERIMENTAL SECTION

2.1. Materials

a) Chemicals

For SAM formation and activation: 11-mercaptoundecanoïc acid (MUA), N-hydroxysuccinimide (NHS) and 1-(3-dimethylaminopropyl)-N'-ethylcarbodiimide hydrochloride (EDC) were purchased from Sigma Aldrich and used as received.

$(NBu_4)_3$ $[PW_{11}O_{39}((SiC_6H_4NH_2)_2O)]$ was prepared following the procedure we previously described.[46] *p*-Aminophenyltrimethoxysilane and tetrabutylammonium bromide were purchased from Acros Organics and used as received. Solvents and acids were obtained from various commercial sources.

Protein adsorption and reactivity: Secondary anti-rabbit IgG's (anti-rIgG) were kindly provided by P.G. Marnet from INRA-Rennes. PBS (phosphate-buffered saline, pH=7.4), Bovin Serum Albumin (BSA) and rabbit IgG (anti-rIgG) were purchased from Sigma Aldrich.

All solvents were reagent-grade, used without any further purification. Experiments were carried out at room temperature if not specified otherwise.

For spectroscopic analyses and AFM images, the surfaces, constituted of glass substrates (11mm×11 mm) coated successively with a 5 nm thick layer of chromium and a 200 nm thick layer of gold, were purchased from Arrandee (Werther, Germany). The gold-coated substrates were annealed in a butane flame to ensure a good crystallinity of the topmost layers and rinsed in a bath of absolute

ethanol during 15 minutes before adsorption. After annealing, these substrates are expected to display large (111)-oriented large terraces. Quartz Crystal Microbalance measurement were done using AT-cut 5 MHz quartz crystals coated with a 3-100 nm thick layer of gold (Lot-oriel, Massy, France). Before use, they were cleaned by ethanol and dried under nitrogen flow.

b) Self assembled monolayer formation and POM grafting

- Acid terminated layers: Gold substrates were immersed in 10 mL of 1 mM solution of MUA in absolute ethanol for 18h and were rinsed in absolute ethanol (2×5 min). Then substrates were dried under a flow of dry nitrogen.

- Activation procedure: The substrates were treated by depositing a 150 µL drop of a solution of NHS (2.4 eq) and EDC (1.2 eq) in Milli-Q water for 2 hours, were rinsed with milli-Q water and were dried under a flow of dry nitrogen.

- POM immobilization: POM immobilization was achieved through the reaction of its amine group with the previously activated layer of MUA. To establish the best experimental conditions of POM immobilisation, the activated substrates were immersed in a 10 mL solution of POMs in different solvents (acetone, acetonitrile or dimethylformamide), and rinsed three times in the same solvents. Various concentrations of POMs, in the range 0.5 to 5 mM and various immersion times (from 2 to 18 hours) have been tested.

c) Protein grafting and molecular recognition

Secondary monoclonal antibodies, anti-rIgGs, (50 $mg.L^{-1}$ in PBS) were activated for 1h30 by a solution of NHS (2.2 eq) and EDC (1.1 eq) in PBS buffer. Substrates (IR and quartz sensors) were treated for 20 min (time taken to the QCM curve stabilization) with the activated antibody solution and rinsed with a PBS (phosphate-buffered saline, pH = 7.4) buffer. The immobilized antibody was then contacted with a 50 $mg.L^{-1}$ solution of BSA for 20 min and rinsed with PBS. Eventually, sensors were exposed to a 50 $mg.L^{-1}$ solution of rabbit IgG in PBS.

2.2. Techniques

PM-IRRAS: PM-IRRAS spectra were recorded on a commercial Thermo-scientific (France) Nexus spectrometer. The experimental setup has been described previously.[47]

XPS: XPS analyses were performed using a PHOIBOS 100 X-ray photoelectron spectrometer from SPECS GmbH (Berlin, Germany with the monochromatic Al-Kα X-ray source (hν = 1486.6 eV) operating at 10^{-10} Torr or less. The conditions for high-resolution XPS were determined for a "Fixed Analyser Transmission" analysis mode, i.e., a 7× 20 mm entrance slit, leading to a resolution of 0.1 eV for the spectrometer, and an electron beam power of 150 W (12.5 kV and 12 mA). The angle of collection was 90° with respect to the sample plane. Element peak intensities were corrected

by Scofield factors and spectra were fitted using the Casa XPS Software (v.2.3.13, Casa software Ltd. UK). A pseudo-Voigt function with a Gaussian/Lorentzian ratio equal to 70/30 was used to decompose photopeaks.

AFM: AFM measurements were done using Veeco NanoScope® Multimode VI using oxide-sharpened microfabricated Si_3N_4 cantilevers (Microlevers, Veeco Metrology LLC, Santa Barbara, CA) with a spring constant of 0.36 N/m. Images were recorded under air, at room temperature, in Peak Force Tapping™ mode, newly developed and described in reference.[20] All images shown in this paper are flattened raw data.

QCM-D: Piezoelectric measurements were carried out with a dissipative quartz crystal microbalance (QSense, Sweden). Experiments were carried out in dynamic conditions using a peristaltic pump operating at a flow of 50 µL/min. Data were simultaneously acquired at the fundamental frequency F of 5 MHz (N = 1) and several overtone frequencies (15, 25, 35, 45, and 55 MHz, i.e. N = 3, 5, 7, 9 and 11) For clarity, only the fifth harmonic data are shown. Two physical parameters are discussed: the frequency of oscillation and the dissipation that increases with the adsorbed mass when the adsorbed layer is not rigid. The dissipation evolution was used to check the validity of the Sauerbrey model, that enables to correlate the frequency change to the mass of the adsorbed layer when the dissipation change is low, using the following equation[16]:

$\Delta F = - N \Delta m / C_f$,

where C_f (= 17.7 ng cm^{-2}·Hz at F = 5 MHz) is the mass-sensitivity constant, and N is the overtone number.

3. RESULTS AND DISCUSSION

- Optimizing POM grafting on the acid terminated layer

The nanostructured layer was built stepwise, starting with an acid-terminated self assembled monolayer (SAM) of mercaptoundecanoic acid (MUA) on gold, followed by its activation prior to the covalent grafting of the $(NBu_4)_3$ $[PW_{11}O_{39}\{(SiC_6H_4NH_2)_2O\}]$ polyoxometalate (POM). The interest of using a POM bearing two amine functions is twofold: first, it enables the covalent grafting of the POM on the acid-terminated SAM; second, it is expected to lead to a regular pattern of amine functions distributed over the surface, available for the further grafting of biomolecular probes. The risk is obviously the grafting of the POM through both amine functions preventing further reaction with biomolecules, thus reinforcing the relevance of PM-IRRAS characterization to check the presence of free terminal amine functions. Several experimental parameters (solvent nature, immersion time and concentration of the POM solution) have been explored. Among the tested solvents, acetonitrile led to the most efficient grafting compared to acetone or dimethylformamide.

The results discussed below have all been obtained using acetonitrile as solvent for POM- involving reactions, and rinsing.

Figure 2

The PM-IRRAS spectra obtained at each step of gold surface functionalization are shown in Figure 2. The formation of an acid-terminated SAM on gold surfaces (Figure 2.a) is evidenced by the appearance of the asymmetric and symmetric COO^- stretching vibrations bands at 1585 and 1440 cm^{-1}, together with a shoulder to the former one, associated to the C=O stretching vibrations at 1715 cm^{-1}. The asymmetric and symmetric CH_2 stretching and deformation vibrations bands of MUA are also present at 2927, 2853 and 1457 cm^{-1}. After activation of the terminal acid groups by *N*-hydroxysuccinimide (NHS) and 1-(3-dimethylaminopropyl)-N'-ethylcarbodiimide hydrochloride (EDC), new IR absorption bands appear (Figure 2.b): the carbonyl stretching vibration of the O=C-O-NR group at 1741 cm^{-1} and the carbonyl stretching vibrations of the succinimide at 1817 and 1787 cm^{-1}. Simultaneously, the carbonyl vibration band of the carboxylic acids decreases. All these features confirm the activation of the O=C-OH, or COO^- terminal functions into O=C-O-NR group, highly reactive towards amine groups. The spectrum obtained upon reaction of the activated SAM with a solution of POMs is shown in (Figure 2c). Several spectral features prove the successful grafting of POM: first, the decrease of the ester bands, at 1741, 1787 and 1817 cm^{-1} which indicates their reaction with POMs; second, the presence of characteristic amide bands at 1655 cm^{-1} (amide I) and 1545 cm^{-1} (amide II) indicates the formation of an amide bond between the activated surface acid groups and POM amino groups. The signatures of the POMs are also observed at 970 cm^{-1} (νW-O), 1067 cm^{-1} (νP-O), 1110 cm^{-1} (νSi-O), 1598 cm^{-1} ($\nu C=C_{ar}$), and 1630 cm^{-1} (δN-H). It is worth noting the presence of an IR absorption band at 1630 cm^{-1}, reasonably attributed to the N-H deformation vibration, which indicates that part of the amine groups have not reacted with surface acid functions. These amine groups of POM are therefore left available for further grafting; this will be subsequently confirmed by their reaction with the biomolecules.

On the other hand, the band at 1741 cm^{-1} due to the carbonyl stretching vibrations of the activated acid groups is still visible, showing that some acid groups from the MUA SAM have not reacted. This result can be easily explained by the relative sizes of MUA (a few tenths of nm distance between two successive MUA) and the selected POM (1 nm approx. in diameter), which, upon reaction with one activated MUA will "cover" its neighbors hindering their reaction with another POM; this will be discussed in detail and quantified further below, on the basis of XPS data.

Varying POM concentration in the acetonitrile solution (from 0.5 to 5 mM) led to similar PM-IRRAS signatures, peak intensities increasing linearly with the POM concentration, not enabling to

determine the optimal concentration for POM grafting. Therefore, the dispersion of POMs adsorbed on gold surfaces starting from various concentrations was studied by AFM. The images of the acid-terminated layers obtained before and after immobilization of the POMs, using either 1 mM or 0.5 mM solutions, together with the MUA layer prior to POM grafting, are shown in **Figure 3**.

Figure 3

Images of the MUA layer are very flat with a sub-nanometric roughness indicating the formation of a dense and relatively ordered monolayer of MUA. Upon POM grafting, starting from a 1 mM solution (**Figure 3**-b), images show a dense and well dispersed layer of POM clusters on the surface. In some regions, few aggregates can be observed. The cross section indicates that these aggregates (~ 3 nm in height) correspond likely to clusters of 2 ~ 3 POMs, however, we can consider that the overall dispersion was satisfying. Using a less concentrated solution (0.5 mM) improved the dispersion of POMs on the gold layer (**Figure 3**-c). Indeed, the formed layer is still dense but very few aggregates can be observed. On the cross section, the maximum height of 1.5 nm proves the presence of a single layer of organized POMs; even though the lateral resolution of AFM did not enable discriminating clusters from single POMs, the 2D arrangement seems regular. Therefore, one can assume that only the covalently grafted POMs were retained on the surface. Note that the presence of ligands (see XPS data) may also explain the POM dispersion.
On the basis of these results, the concentration of 0.5 mM was chosen for POM immobilization on the acid activated SAM, and further immobilization of proteins.

- XPS characterization of the POM layer

Once the optimal conditions of POM grafting established, from AFM and PM-IRRAS data, the layers were fully characterized and the surface coverage estimated using XPS. The results are shown in Figure 4.
The POM grafting is evidenced by XPS features at 37, 248, 428, and 400 eV, easily attributed to W4f, W4d, W4p, and N1s levels, respectively (Fig.4a). This is confirmed by an attenuation of the Au4f and S2p peaks (not shown). The W4f peak (Fig.4a) is composed of a well resolved spin-orbit doublet (36.2 and 38.4 eV for $W4f_{7/2}$ and $W4f_{5/2}$, respectively) typical of W(VI) atoms and in agreement with literature data on deposited Keggin-type POMs.[48] Note that, when recording the W4f signals again, at the end of the XPS analysis, the W4f peak displayed additional contributions at 35.2 and 37.2 eV (Fig.4b), that we have attributed to a partial reduction of tungsten under X-ray irradiation. Such a split of the W doublet has already been observed for Keggin-type molybdenum heteropolyacids ($H_3PMo_{12}O_{40}$) and ascribed to two different molybdenum states.[49]. Similar

shoulders have been attributed by other authors to tungsten atoms in direct contact with the surface,[50] or explained by the presence of water.[51] Since it is time dependent, we rather think that it is simply matter of reduction during X-ray irradiation. It is thus essential to record the W 4f peaks prior to the other ones.

Figure 4

Figures 4-c and d show the O1s peaks of the MUA and MUA+POM/Au. The entire XPS analysis of the MUA/Au layer is in agreement with that reported in literature.[52] The O1s peak after POM grafting could be reasonably decomposed into 3 components. The contribution at lower binding energy, 531.4 eV, is attributed to oxygen bound to W, P or Si (Si-O-Si, W-O-W, W-O-P and W=O bonds); there is probably a subtle distinction between these several types of oxygen, which we prefer not to assess from the measured XPS peak. The components at 532.7 and 533.7 eV can be attributed to the oxygen atoms of the activated MUA terminal functions (C=O, and C-O-N respectively). These binding energy values are slightly higher (+1 eV), than the values observed for MUA or similar organic compounds; we tentatively explained it by a lowering of the electron density in C=O and C-O-N bonds in the vicinity of the electron-rich POMs. Note also that there may be some residual water, which would contribute to a high energy shift. From the O1s peak, it is also possible to determine the number of MUA molecules that have reacted with POMs. The O_{POM}/O_{MUA} ratio, determined by dividing the contribution at 531.4 eV by the sum of the contributions at 532.7 and 533.7 eV, is equal to 0.9 (expected O_{POM}/O_{MUA} ratio equal to 10 for one activated MUA per one POM). Thus, about one out of 11 acid functions has formed an amide bond with a POM anion.

A bilayer model has been used to determine the MUA (d1) and POM (d2) layer thicknesses. The equations correlating photopeak intensities (Au4f and O1s) to the two thickness values are given below (equations 1, 2 and 3) [53]:

$$I_O(POM) = n_O(POM)\sigma_{O1s}T_{O1s}\lambda_{O1s}^{POM}\left(1 - exp\left(\frac{-d_2}{\lambda_{O1s}^{POM}}\right)\right) \quad \textbf{(1)}$$

$$I_O(MUA) = n_O(MUA)\sigma_{O1s}T_{O1s}\lambda_{O1s}^{MUA}\left(1 - exp\left(\frac{-d_1}{\lambda_{O1s}^{MUA}}\right)\right)exp\left(\frac{-d_2}{\lambda_{O1s}^{POM}}\right) \quad \textbf{(2)}$$

$$IAu = n_{Au}\sigma_{Au4f}T_{Au4f}\lambda_{Au4f}^{Au}exp\left(\frac{-d_1}{\lambda_{Au4f}^{MUA}}\right)exp\left(\frac{-d_2}{\lambda_{Au4f}^{POM}}\right) \quad \textbf{(3)}$$

where $I_O(POM)$, $I_O(MUA)$ and I_{Au} are the intensities of the corresponding components of the O1s peak and the Au4f peak intensity, n_O and n_{Au} are the oxygen and gold mole numbers per cm^3,

σ_{O1s} and σ_{Au4f} are the photoionization cross sections of the O1s and Au4f electrons, T_{O1s} and T_{Au4f} are the transmission factors, $\lambda_{O1s}^{POM}, \lambda_{O1s}^{MUA}, \lambda_{Au4f}^{POM}, \lambda_{Au4f}^{MUA}$ *and* λ_{Au4f}^{Au} are the attenuation lengths of the O1s and Au4f electrons in the POM, MUA and substrate layer respectively[54]. The thicknesses of the POM, and of the activated MUA layers have been estimated to 0.9 and 1.5 nm respectively, consistently with the formation of successive monolayers.

The estimated thickness of the MUA layer is in agreement with the literature [55,56] and with the above AFM results. As for the POM layer, the calculated thickness is lower than the size (1.0 - 1.2 nm) of $H_nXW_{12}O_{40}$ (X=P, Si, B, Co) determined by X-Ray crystallography.[57] This could be explained either by taking into account that the calculated thickness is an average, comprising the surface areas free of POMs, or considering that the POM can be tilted when grafted to the MUA layer. However, our results tend to indicate that a complete, or almost complete, monolayer of POMs has indeed been formed.

Last but not least, the N 1s peak, displayed on Fig. 4-e, shows three contributions at 398.9, 400.5 and 402.6 eV, reasonably attributed to nitrogen in C-N, NH_2 and $C\text{-}N^+$ groups respectively. The first one is obviously originating from the just created amide groups, the second one from the amine groups of the POM, while the last one is related to the tetrabutylammonium conterions.

- Protein immobilization and recognition test

The POM-based nanostructured surface was eventually applied to the elaboration of a nanostructured biosensor, whose efficiency was then tested. In a first stage, a secondary anti-rabbit immunoglobulin (anti-rIgG) was reacted with the free amine groups of the bifunctional polyoxometalate, in order to link them in a covalent way. Then the specific recognition of rabbit immunoglobulin (rIgG), and the non specific binding of BSA, were assessed. The successive steps of protein grafting and recognition were monitored *ex-situ* by PM-IRRAS, and *in-situ* using quartz crystal microbalance with dissipation measurements (QCM-D). The presence of intense amide bands on the PM-IRRAS spectra (not shown) proved the efficient grafting of proteins. QCM-D curves, i.e., the frequency and dissipation changes measured at the fifth harmonic, are shown in Figure 5. Injections of protein solutions and of PBS buffer are indicated with arrows on the figure.

Figure 5

The frequency variations measured by QCM after rinsing and the corresponding mass values, calculated by using the Sauerbrey equation, are presented in the Table 1.

Table 1: Measured frequency variations after rinsing and calculated equivalent mass

	Frequency variation (Hz)	Equivalent mass (µg/cm²)
Anti IgG	29.1	0.52
BSA	0.6	0.01
IgG	32.4	0.58

Upon injection of an anti-rIgG solution, one observes a frequency decrease of 29.1 Hz. This indicates the strong binding of anti-rIgG to the surface. The corresponding dissipation (upper curve in Figure 5) was very low suggesting the formation of a densely packed layer of proteins, thus validating the Sauerbrey equation to determine the mass uptake. The estimated mass of bound anti-rIgG, is 515 ng/cm², corresponding to 3.4 pmol/cm². The expected value for a full monolayer of anti-rIgG is comprised between 1.2 and 2.5 pmol/cm².(ref[6] and references therein) We thus assume that the surface is indeed fully covered by the antibodies. The excess in the experimental mass could be explained by water molecules trapped within the layer, which may indeed double the estimated mass of the protein layer [58,59]. Upon BSA injection, a slight decrease in frequency (0.6 Hz) was recorded, indicating that non specific adsorption is very weak. The quality of the anti-rIgG layer, allowing very little unspecific interactions confirms the full coverage of adsorption sites, probably due to the regular organization of POMs on the surface. Eventually, injection of the specific target, rIgGs, induced a decrease of the frequency to 32.4 Hz. At this step, the dissipation increases as expected upon forming a second layer of protein, but the changes are still weak ($2.5\ 10^{-6}$) and enabled to apply the Sauerbrey equation, leading to a mass uptake of 573 ng/cm², which corresponds to an rIgG/ anti-rIgG molecular ratio equal to 1.1. Taking into account the geometric hindrance very likely to occur within a dense anti-rIgG layer, this value is more than satisfying [6,47] and proves the efficiency of the POM-structured biosensor for both recognizing a specific target and avoiding non specific interactions. At this stage, we must admit that a rather large protein has been chosen for testing the new nanostructured surface with the objective of comparing its immobilization and recognition capacities to those we previously used.[6] Of course, once validated, more relevant results will be expected when we graft a small molecular probe, such as a toxin on a surface, whose structuring scale is of the order of some tenths of nanometers. Such experiments are in progress. For this kind of target, the detection is often done in a competitive or indirect format.[47,60] In this format, the target is immobilized on the surface and its presence in a media is evidenced by a decrease in the number of bound proteins. Therefore, the accessibility and reproducibility of the immobilized species are even more crucial.

4. CONCLUSION

A densely packed, nanostructured surface has been elaborated by coupling an activated acid-terminated alkylthiol self-assembled monolayer on gold with an organosilyl-derivatized POM,

bearing two pendant amine functions oriented in opposite directions. The conditions enabling the formation of a well dispersed layer of amine terminated-POMs were determined using PM-IRRAS, AFM, and XPS. The covalent binding of POM to the surface was successfully achieved and led to a structured layer bearing organized amine functions. The resulting POM-nanostructured layer was then successfully used to immobilize proteins, resulting in a highly specific biorecognition reaction. This new, simple route of surface functionalization has wide applicability in view of the diversity of organically derivatized POMs that can be produced and will be of great interest to build ordered arrays of molecules or proteins to control the efficiency and reproducibility of biorecognition phenomena.

FIGURES CAPTIONS

Figure 1: *Schematic drawing of nanostructured surfaces with polyoxometalates and protein grafting and recognition*

Figure 2: *PM-IRRAS spectra of the gold substrates after: MUA grafting (a), MUA activation (b), POM immobilization (20 h, 5 mM in acetonitrile) (c)*

Figure 3 *AFM images (Peak Force Tapping™ mode, in air;* ***z scale 15 nm****) of gold surfaces covered by MUA (a), POM at 1 mM (b) and 0.5 mM (c).*

Figure 4: *High resolution W4f spectra of the gold surface after POM immobilization, at the beginning (a), and at the end (b) of the XPS analysis; high resolution O1s spectra of the gold surface after MUA grafting(c) and POM immobilization (d)*; *high resolution N1s spectrum after POM immobilization (e)*

Figure 5*: Frequency (bottom curve) and dissipation (upper curve) variation measured during biosensors elaboration and recognition of a rIgG on a POM-functionalized gold quartz surface.*

FIGURES

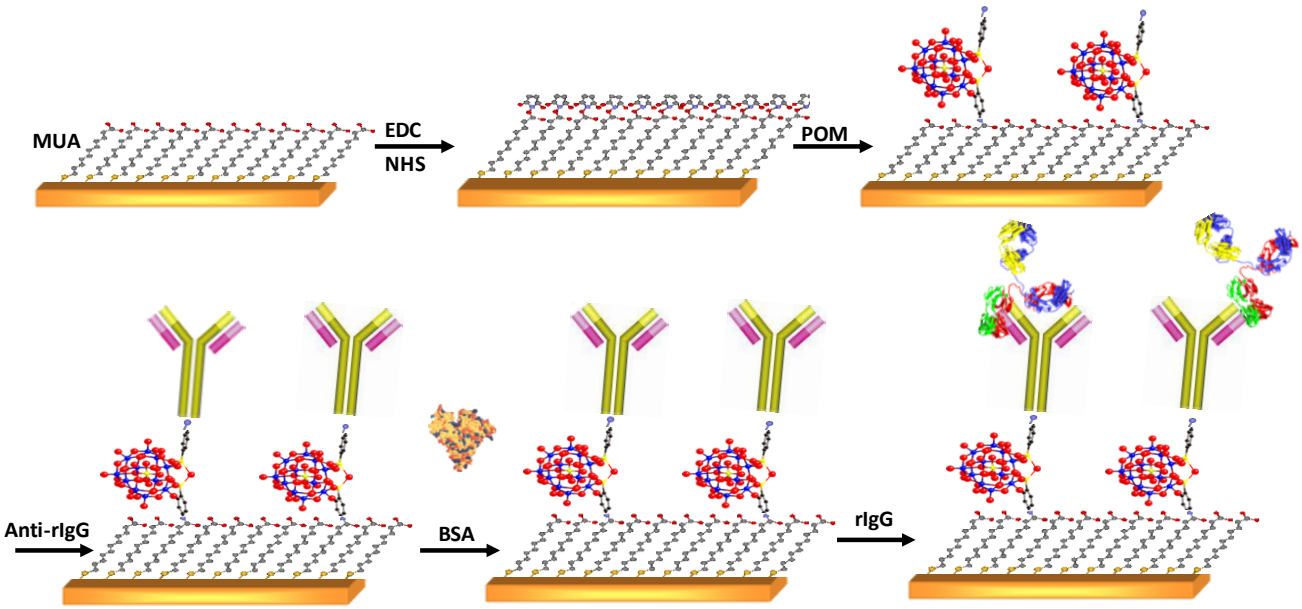

Figure 1: *Schematic drawing of nanostructured surfaces with polyoxometalates and protein grafting and recognition*

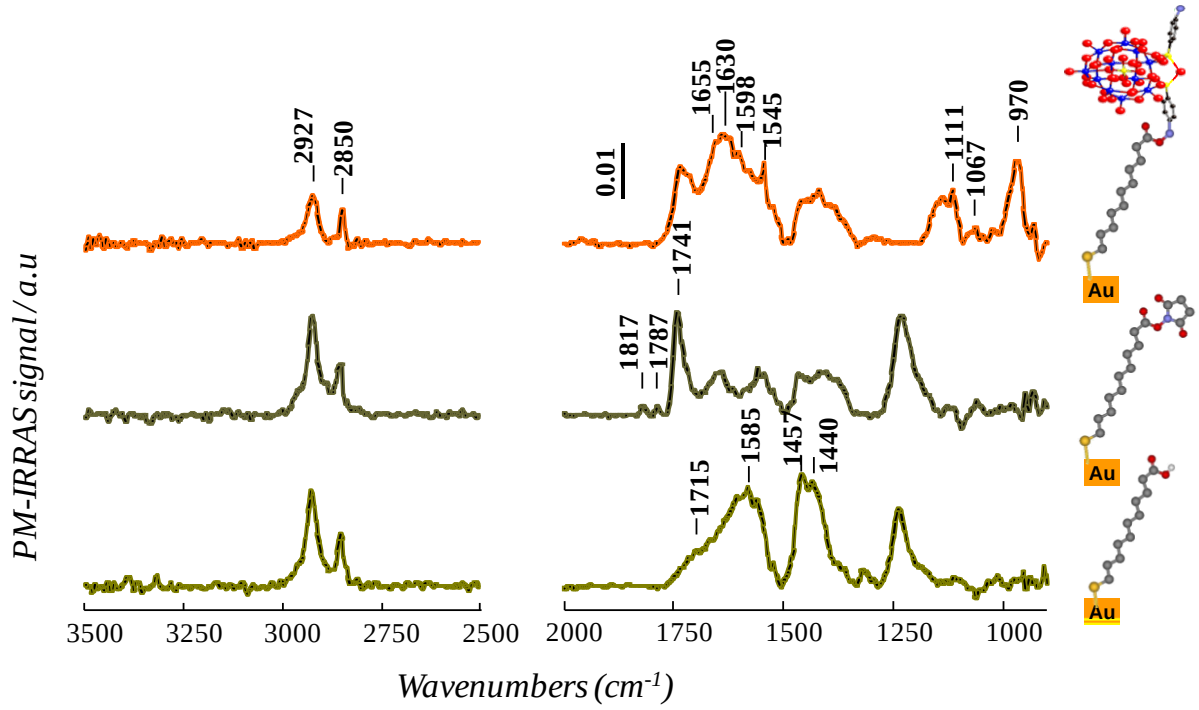

Figure 2: *PM-IRRAS spectra of the gold substrates after: MUA grafting (a), MUA activation (b), POM immobilization (20 h, 5 mM in acetonitrile) (c)*

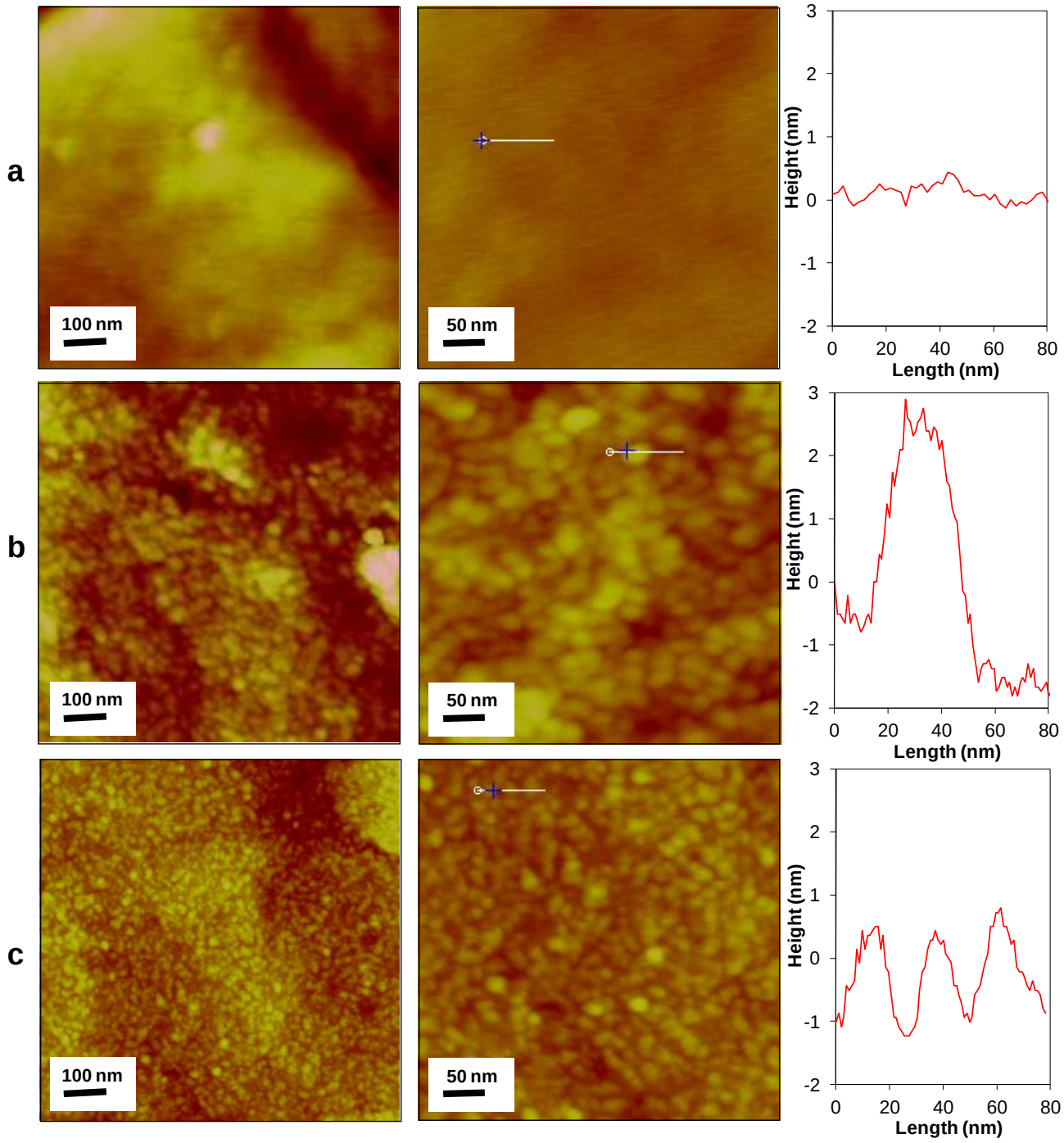

Figure 3 *AFM images (Peak Force Tapping™ mode, in air;* ***z scale 15 nm****) of gold surfaces covered by MUA (a), POM at 1 mM (b) and 0.5 mM (c).*

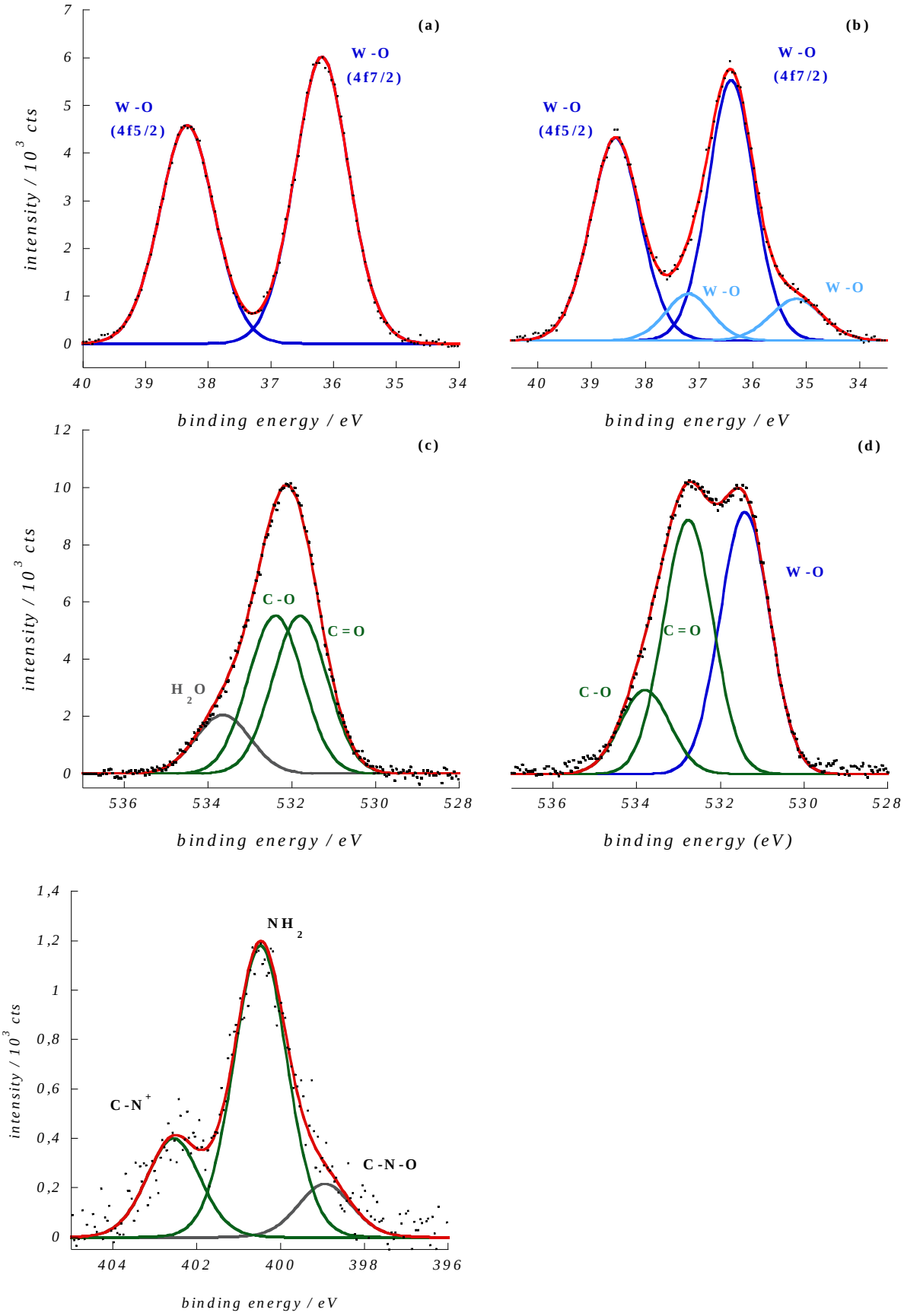

Figure 4: *High resolution W4f spectra of the gold surface after POM immobilization, at the beginning (a), and at the end (b) of the XPS analysis; high resolution O1s spectra of the gold surface after MUA grafting(c) and POM immobilization (d); high resolution N1s spectrum after POM immobilization (e)*

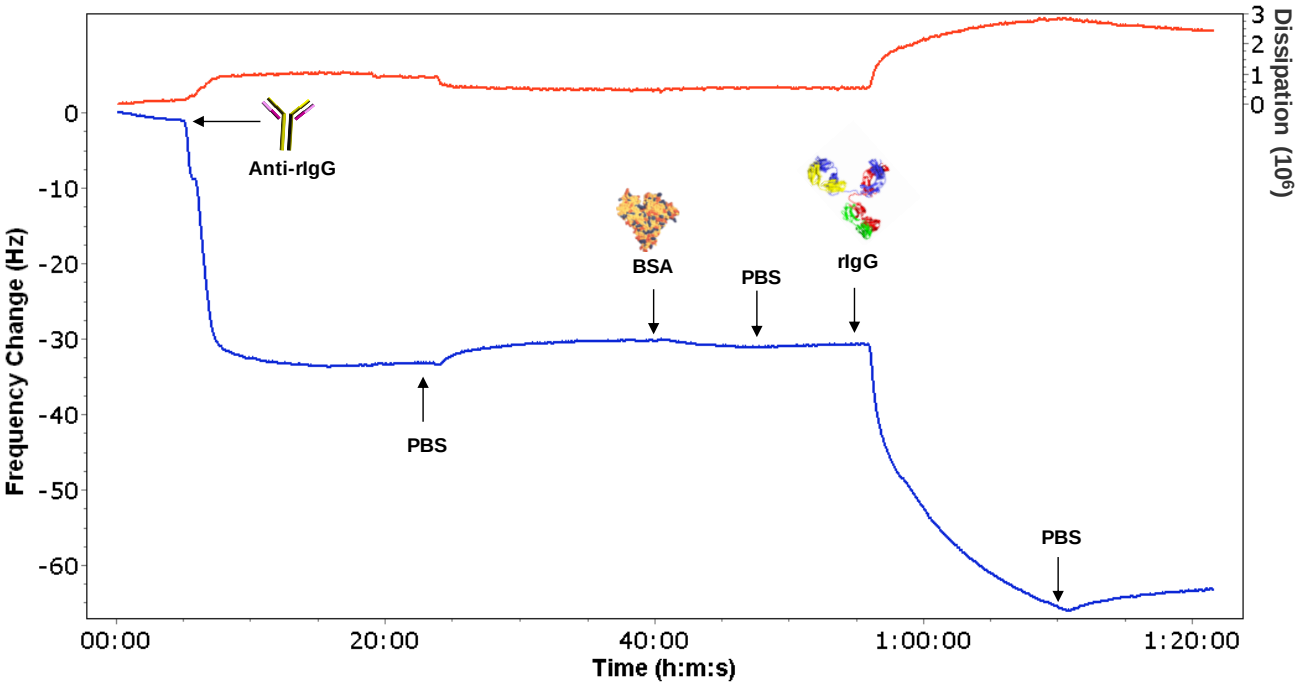

Figure 5*: Frequency (bottom curve) and dissipation (upper curve) variation measured during biosensors elaboration and recognition of a rIgG on a POM-functionalized gold quartz surface.*

REFERENCES

(1) Lazcka, O.; Del Campo, F. J.; Munoz, F. X. *Biosensors and Bioelectronics* **2007**, *22*, 1205.

(2) Mirsky, V. M.; Riepl, M.; Wolfbeis, O. S. *Biosensors \& Bioelectronics* **1997**, *12*, 977.

(3) Ulman, A. *Chemical Reviews* **1996**, *96*, 1533.

(4) Gooding, J. J.; Mearns, F.; Yang, W. R.; Liu, J. Q. *Electroanalysis* **2003**, *15*, 81.

(5) Griveau, S.; Mercier, D.; Vautrin-Ul, C.; Chaussé, A. *Electrochemistry Communications* **2007**, *9*, 2768

(6) Boujday, S.; Bantegnie, A.; Briand, E.; Marnet, P.-G.; Salmain, M.; Pradier, C.-M. *Journal of Physical Chemistry B* **2008**, *112*, 6708.

(7) Briand, E.; Gu, C.; Boujday, S.; Salmain, M.; Herry, J. M.; Pradier, C. M. *Surface Science* **2007**, *601*, 3850.

(8) Lu, B.; Smyth, M. R.; Okennedy, R. *Analyst* **1996**, *121*, R29.

(9) Krishnamoorthy, S.; Himmelhaus, M. *Advanced Materials* **2008**, *20*, 2782+.

(10) Boujday, S.; Briandet, R.; Salmain, M.; Herry, J.-M.; Marnet, P.-G.; Gautier, M.; Pradier, C.-M. *Microchimica Acta* **2008**, *163*, 203.

(11) Zhu, H.; Yan, J.; Revzin, A. *Colloids and Surfaces B: Biointerfaces* **2008**, *64*, 260.

(12) Lalander, C. H.; Zheng, Y.; Dhuey, S.; Cabrini, S.; Bach, U. *ACS Nano* **2010**, *4*, 6153.

(13) Lee, K. B.; Kim, E. Y.; Mirkin, C. A.; Wolinsky, S. M. *Nano Letters* **2004**, *4*, 1869.

(14) Lee, S. W.; Oh, B. K.; Sanedrin, R. G.; Salaita, K.; Fujigaya, T.; Mirkin, C. A. *Advanced Materials* **2006**, *18*, 1133+.

(15) Corbierre, M. K.; Beerens, J.; Beauvais, J.; Lennox, R. B. *Chemistry of Materials* **2006**, *18*, 2628.

(16) Xu, S.; Miller, S.; Laibinis, P. E.; Liu, G. Y. *Langmuir* **1999**, *15*, 7244.

(17) Baralia, G. G.; Pallandre, A.; Nysten, B.; Jonas, A. M. *Nanotechnology* **2006**, *17*, 1160.

(18) Morel, A.-L.; Boujday, S.; Méthivier, C.; Krafft, J.-M.; Pradier, C.-M. *Talanta* **2011**, *85*, 35.

(19) Morel, A.-L.; Volmant, R.-M.; Méthivier, C.; Krafft, J.-M.; Boujday, S.; Pradier, C.-M. *Colloids and Surfaces B: Biointerfaces* **2010**, *81*, 304.

(20) Spadavecchia, J.; Boujday, S.; Landoulsi, J.; Pradier, C. M. *ACS Applied Materials & Interfaces* **2011**, null.

(21) Pope, M. T.; Muller, A. *Angewandte Chemie-international Edition In English* **1991**, *30*, 34.

(22) Long, D. L.; Tsunashima, R.; Cronin, L. *Angewandte Chemie-international Edition* **2010**, *49*, 1736.

(23) Hill, C. L. *Chemical Reviews* **1998**, *98*, 1.

(24) T. Yamase, M. T. P. *Polyoxometalate chemistry for Nano-composite Design*; Kluwer Academic/Plenum Publishers, 2002.

(25) Long, D. L.; Burkholder, E.; Cronin, L. *Chemical Society Reviews* **2007**, *36*, 105.

(26) Proust, A.; Thouvenot, R.; Gouzerh, P. *Chemical Communications* **2008**, 1837.

(27) Clemente-Leon, M.; Coronado, E.; Gomez-Garcia, C. L.; Mingotaud, C.; Ravaine, S.; Romualdo-Torres, G.; Delhaes, P. *Chemistry-a European Journal* **2005**, *11*, 3979.

(28) Liu, S. Q.; Volkmer, D.; Kurth, D. G. *Analytical Chemistry* **2004**, *76*, 4579.

(29) Qi, W.; Li, H. L.; Wu, L. X. *Journal of Physical Chemistry B* **2008**, *112*, 8257.

(30) Rosnes, M. H.; Musumeci, C.; Pradeep, C. P.; Mathieson, J. S.; Long, D. L.; Song, Y. F.; Pignataro, B.; Cogdell, R.; Cronin, L. *Journal of the American Chemical Society* **2010**, *132*, 15490.

(31) Liu, S. Q.; Kurth, D. G.; Volkmer, D. *Chemical Communications* **2002**, 976.

(32) Turdean, G. L.; Curulli, A.; Popescu, I. C.; Rosu, C.; Palleschi, G. *Electroanalysis* **2002**, *14*, 1550.

(33) Errington, R. J.; Petkar, S. S.; Horrocks, B. R.; Houlton, A.; Lie, L. H.; Patole, S. N. *Angewandte Chemie-international Edition* **2005**, *44*, 1254.

(34) Joo, N.; Renaudineau, S.; Delapierre, G.; Bidan, G.; Chamoreau, L. M.; Thouvenot, R.; Gouzerh, P.; Proust, A. *Chemistry-a European Journal* **2010**, *16*, 5043.

(35) Song, Y. F.; McMillan, N.; Long, D. L.; Kane, S.; Malm, J.; Riehle, M. O.; Pradeep, C. P.; Gadegaard, N.; Cronin, L. *Journal of the American Chemical Society* **2009**, *131*, 1340.

(36) Alam, M. S.; Dremov, V.; Muller, P.; Postnikov, A. V.; Mal, S. S.; Hussain, F.; Kortz, U. *Inorganic Chemistry* **2006**, *45*, 2866.

(37) Kaba, M. S.; Song, I. K.; Duncan, D. C.; Hill, C. L.; Barteau, M. A. *Inorganic Chemistry* **1998**, *37*, 398.

(38) Song, I. K.; Kaba, M. S.; Nomiya, K.; Finke, R. G.; Barteau, M. A. *Journal of Molecular Catalysis A: Chemical* **2007**, *262*, 216

(39) Tang, Z.; Liu, S.; Wang, E.; Dong, S. *Langmuir* **2000**, *16*, 4946.

(40) Zhong, D. Y.; Sousa, F. L.; Muller, A.; Chi, L. F.; Fuchs, H. *Angewandte Chemie-International Edition* **2011**, *50*, 7018.

(41) Keita, B.; Nadjo, L. *J. Mol. Catal.* **2007**, *262*, 190.

(42) Musumeci, C.; Luzio, A.; Pradeep, C. P.; Miras, H. N.; Rosnes, M. H.; Song, Y. F.; Long, D. L.; Cronin, L.; Pignataro, B. *Journal of Physical Chemistry C* **2011**, *115*, 4446.

(43) Dolbecq, A.; Dumas, E.; Mayer, C. R.; Mialane, P. *Chemical Reviews* **2010**, *110*, 6009.

(44) Duffort, V.; Thouvenot, R.; Afonso, C.; Izzet, G.; Proust, A. *Chemical Communications* **2009**, 6062.

(45) Villanneau, R.; Racimor, D.; Messner-Henning, E.; Rousseliere, H.; Picart, S.; Thouvenot, R.; Proust, A. *Inorganic Chemistry* **2010**, *50*, 1164.

(46) Matt, B.; Renaudineau, S.; Chamoreau, L. M.; Afonso, C.; Izzet, G.; Proust, A. *Journal of Organic Chemistry* **2011**, *76*, 3107.

(47) Boujday, S.; Gu, C.; Girardot, M.; Salmain, M.; Pradier, C.-M. *Talanta* **2009**, *78*, 165.

(48) Legagneux, N.; Basset, J. M.; Thomas, A.; Lefebvre, F.; Goguet, A.; Sa, J.; Hardacre, C. *Dalton Transactions* **2009**, 2235.

(49) Grinenval, E.; Basset, J. M.; Lefebvre, F. *Inorganica Chimica Acta* **2011**, *370*, 297.

(50) Newman, A. D.; Brown, D. R.; Siril, P.; Lee, A. F.; Wilson, K. *Physical Chemistry Chemical Physics* **2006**, *8*, 2893.

(51) Jalil, P. A.; Faiz, M.; Tabet, N.; Hamdan, N. M.; Hussain, Z. *Journal of Catalysis* **2003**, *217*, 292.

(52) Tielens, F.; Costa, D.; Humblot, V.; Pradier, C. M. *Journal of Physical Chemistry C* **2008**, *112*, 182.

(53) Maurice, V.; Despert, G.; Zanna, S.; Josso, P.; Bacos, M. P.; Marcus, P. *Surface Science* **2005**, *596*, 61.

(54) Tanuma, S.; Powell, C. J.; Penn, D. R. *Surface and Interface Analysis* **1994**, *21*, 165.

(55) Evans, S. D.; Ulman, A.; Goppert-Berarducci, K. E.; Gerenser, L. J. *Journal of the American Chemical Society* **1991**, *113*, 5866.

(56) Frey, B. L.; Jordan, C. E.; Kornguth, S.; Corn, R. M. *Analytical Chemistry* **1995**, *67*, 4452.

(57) Kim, G. S.; Hagen, K. S.; Hill, C. L. *Inorganic Chemistry* **1992**, *31*, 5316.

(58) Hook, F.; Kasemo, B.; Nylander, T.; Fant, C.; Sott, K.; Elwing, H. *Analytical chemistry* **2001**, *73*, 5796.

(59) Hook, F.; Rodahl, M.; Brzezinski, P.; Kasemo, B. *Langmuir* **1998**, *14*, 729.

(60) Boujday, S.; Nasri, S.; Salmain, M.; Pradier, C.-M. *Biosensors and Bioelectronics* **2010**, *26*, 1750.